Structure and rheology of carboxymethylcellulose in polar solvent mixtures

Can Hou[a], Takaichi Watanabe[b], Carlos G. Lopez[a,c], Walter Richtering[a,d]

[a]*Institute of Physical Chemistry, RWTH Aachen University, Landoltweg 2, Aachen, 52074, Germany, European Union*
[b]*Okayama University, Department of Applied Chemistry, Graduate School of Natural Science, Okayama, 700-8530, Japan*
[c]*Current address: Material Science and Engineering departments, The Pennsylvania State University, 1 Pollock Rd, State College, 16801, PA, US*
[d]*DWI - Leibniz-Institut fur Interaktive Materialien, RWTH Aachen University, Forckenbeckstraße 50, Aachen, 52074, , Germany, European Union*

Abstract

We study the conformational, conductometric and rheological properties of semiflexible polyelectrolyte carboxymethyl cellulose in mixtures of water and three non-solvents (ethanol, isopropanol and acetone). Small angle x-ray scattering measurements of the correlation length reveal that the local conformation of the carboxymethyl chain is largely unchanged by the presence of a non-solvent, even for solutions not far from the phase boundary. Rheological measurements confirm the invariance of the correlation length upon non-solvent addition. Conductivity measurements show that as the non-solvent content is increased, the fraction of condensed counterions increases, presumably due to the lowering of the dielectric constant of the solvent media. These results therefore show that under the conditions studied here, the conformation of polyelectrolyte chains is largely independent of the effective charge fraction of the backbone. We suggest this occurs because the bare Kuhn length ($\simeq 10$ nm) is much larger than electrostatic blob size ($\simeq 1-2$ nm).

Keywords: polyelectrolyte, rheology, scattering, carboxymethyl cellulose

1. Introduction

Polyelectrolytes are widely used as rheology enhancers in the food products, cosmetics Savary et al. (2016); Lochhead et al. (2017) and pharmaceu-

tical formulations.Lankalapalli and Kolapalli (2009); Dakhara and Anajwala (2010) Their good solubility in aqueous media underpins many of the industrial and biological roles. Böhm and Kulicke (1997) By contrast, many common polyelectrolytes are insoluble in organic solvents such as alcohols or ketones. Polyelectrolytes are often used in water-based products which incorporate other solvents. For example, wines, where polyelectrolyte are used to prevent tartaric acid crystallisation typically contain 10-15% ethanol by volume,Bajul et al. (2017) in pharmaceutical creams, which incorporate glycerol as a humectant and in hand sanitisers, which consist of 70-80% alcohol (usually ethanol or 2-propanol, and less frequently 1-propanol).Silva et al. (2022)

The solubility of polyelectrolytes in salt-free liquids markedly differs from that of non-ionic polymers. Various theoriesDobrynin et al. (1995); Muthukumar (2002); Dobrynin and Rubinstein (2005) expect that polyelectrolyte solubility in salt-free solvents is controlled by the entropic gain of counterions dissociated from the backbone, and is thus predicted to be nearly independent of the degree of polymerisation of chains. This is in contrast to neutral polymers, where the solubility of the polymer is determined solely by the competition between polymer-solvent interactions and the translational and conformational entropy of the chains. Unfortunately, experimental work on the phase behaviour of polyelectrolyte solutions, remains quite sparse,Eisenberg and Woodside (1962); Eisenberg and Casassa (1960); Eisenberg and Mohan (1959); Prabhu et al. (2003, 2001); Buscall and Corner (1982); Lopez et al. particularly for systems without added salts.

In general, owing to the relatively high dielectric constant of water, the addition of a non-solvent to aqueous polyelectrolyte solutions leads to a lowering of the dielectric constant of the solvent media, which in turn results in a greater fraction of counterions condensing onto the polymer backbone, as expected by the theory of Manning.Manning (1969, 1996) When the solvent quality decreases to a point where the polyelectrolytes approach the phase boundary, chain collapse occurs leading to a steep increase in counterion condensation.Loh et al. (2008) Depending on the solvent properties and concentration range, the approach to the precipitation boundary can be preceded by a sol-gel transition.Komorowska et al. (2017)

The purpose of this paper is to establish the phase behaviour of carboxymethyl cellulose (CMC) in three polar liquid/water mixtures and to investigate its conformational, thermodynamic and flow properties across the full range of the homogeneous phase. By applying a combination of SAXS,

rheology and conductivity measurements, we show that while the addition of a non-solvent promotes counterion condensation, the conformational properties of the CMC chain are largely insensitive to the effective charge of the backbone.

The polymer chosen for this study is carboxymethyl cellulose, a semiflexible cellulose ether, used as a rheology and texture modifier across a wide range of industries.Hollabaugh et al. (1945); Elliot and Ganz (1974); Arancibia et al. (2016); Rodrigues et al. (2020) Carboxymethyl cellulose, commonly used as its sodium salt NaCMC is a semiflexible, weak, strongly charged polyelectrolyte. The chemical composition of the polymer can be characterised by the degree of substitution (DS), which corresponds the number of carboxymethyl groups substituted at the hydroxyl groups of the cellulose backbone. The maximum possible value of DS is 3, but commercial samples typically have DS $\simeq 0.7 - 1.2$.Feddersen and Thorp (1993)

For DS $\gtrsim 1$, carboxymethyl cellulose solutions exhibit 'hydrophilic' behaviour, where interchain associative interactions influence the solution properties only to a small extent, so that thixotropy, gelation and associated rheological phenomena are absent.Lopez et al. (2018) In industrial formulations, such samples are typically described as displaying 'smooth' flow behaviour.DeButts et al. (1957) The solution behaviour of these highly substituted samples in aqueous solutions has been extensively studied and is relatively well understood: scattering experiments show that CMC chains are dispersed at the molecular level, and their rheological properties in semidilute and concentrated solutions can be described by the scaling model.Dürig and Banderet (1950); Lopez et al. (2015, 2017, 2018); Lopez (2020); Behra et al. (2019) Studies have also addressed counterion condensation as a function of polymer concentration and degree of substitution. Ray et al. (2016); Truzzolillo et al. (2009a,b) In water/non-solvent mixtures, earlier experimental work on CMC has focused on conductivity measurementsNandi and Das (2005, 2011); Vink (1982) to quantify the degree of counterion condensation under various solvent conditions and shear and extensional rheology to understand the influence of non-solvent addition on the dynamics of solutions and gels.Jimenez et al. (2020); Komorowska et al. (2017); Wagner et al. (2023); Jimenez et al. (2022)

In the course of this investigation, CMC with a high degree of substitution was used ($DS \simeq 1$). Firstly, the soluble region was established by phase mapping, whereby the soluble range of concentration and solvent mixing ratio was determined by turbidity tests. SAXS measurements were carried out

for samples in the semi-dilute region to determine the correlation length, from which the value for the chain stretch parameter can be extracted. Rheological measurements were carried out to complement the conformational information obtained from SAXS, with a particular emphasis on the semi-dilute non-entangled region, whereby the Flory exponent and the overlap concentration were estimated from fit. The correlation length data were combined with those from conductivity measurements, which were used to estimate the degree of counterion dissociation at different mixing ratios of non-solvents.

2. Experimental Methods

Materials: Deionized (DI) water with a conductivity of $\sim 10^4$ Sm^{-1} was obtained from an Abactus^2 Ultra Pure Water System (Membra Pure Gmbh). Sodium carboxymethylcellulose (NaCMC) with a nominal degree of substitution DS = 1.2 and $M_w = 2.5 \times 10^5$ g/mol was purchased from Sigma Aldrich.The actual DS was estimated by the back-titration procedure described in earlier references to be 0.98.Lopez and Richtering (2019a, 2021) Ethanol and 2-propanol (absolute for analysis EMSURE ACS, ISO, Reag. Ph Eur) of purity greater than 99% were purchased from Sigma-Aldrich. Dialysis membranes with pore sizes 12-14kD were purchased from SpectraPor. For the ion exchange, cesium hydroxide (Sigma Aldrich; 99.9% trace metal basis, 50 wt.% in water) was used. Sodium iodide (ACS reagent $\geq$99.5%) was also procured from Sigma Aldrich.

Preparation of CMC salts: The NaCMC salt was purified by dialysis against DI water to remove excess salts and freeze-dried. The acid form of CMC was prepared by adding HCl to solutions of NaCMC until a pH lower than 2. Solutions were left for at least 24 hrs to homogenise, transferred into dialysis tubing and dialysed against DI water until the conductivity of the bath did not rise beyond 2 $\times 10^{-4}$ S/m. The HCMC was then obtained by freeze-drying. The cesium salt, used for small-angle X-ray scattering experiments, was obtained by dissolving the HCMC in excess CsOH with pH $\gtrsim$ 13 solution followed by dialysis against DI water and freeze frying. The pH was measured using 744 Ph Meter (Metrohm).

Static Light Scattering: SLS measurements were carried out on a a FICA instrument (SLS-Systems). A red laser (λ = 640 nm) and a blue lase (λ = 404 nm) were used. Measurements were carried out in the 20°-150° angular range for the red laser and for 30°-150° for the blue laser, in

both cases, in increments of 5°. The temperature bath was kept at 25 ± 0.1 °C. Cylindrical quartz cuvettes with an diameter of 20 mm were used as scattering cells. These were washed with freshly distilled acetone prior to sample loading. Samples were filtered through 0.1 μm filters, and the first 0.5-1mL of solution was discarded before being loaded into the cells.

Dynamic Light Scattering: DLS experiments were performed on an ALV-CGS3 goniamoeter setup with a LSE-5003 multiple tau correlator. The source a radiation was a 632 nm laser. Samples which had been previously measured on the static light scattering instrument were re-filtered into 10 mm diameter glass cuvettes. Measurements were performed for 30°-150°. The temperature was set to 25.00° ± 0.01 °C.

Small-Angle X-ray Scattering: solutions of CsCMC in ethanol/water, NaCMC in acetone/water and NaCMC in 2-propanol/water mixtures were prepared. Approximately 50 μL of each sample was loaded into 1.5mm-diameter borosilicate capillaries (WJM Glas Müller GmbH) for in-house beamlines, while 2.0mm capillaries also from WJM Glass Müller were used for samples measured at synchrotrons.

The data for each transmission spectrum collected for each sample were averaged across all angles at a given radius from the beam centre by counts per solid angle, then normalised to the incident beam.

Five different sources were used to acquire the scattering spectra for solutions of CsCMC and NaCMC in this study:

- Rigaku SAXS S-Max3000 with a MicroMax002+ X-ray microfocus generator, with the sample placed at 2.6 m from the detector plates; the q-range measured was between 0.05 to 4 nm^{-1}.

- "Ganesha-Air" SAXS system (SAXSLAB, Xenocs), at Forschungszentrum Jülich, Germany. The X-ray source used was a D2-MetalJet (Excillum) with a radiation wavelength of 0.1341 nm, emitted from a liquid-metal anode at a potential of 70 kV with 3.57 mA current. Using a X-ray optic component by Xenocs, the beam was focused to produce a small, high-intensity beam at 55 cm away. The transmitted radiation was recorded by a PILATUS 300K (Dectris) detector, with a q-range of 0.026 to 3 nm^{-1}.

- Nano-inXider (Xenocs) at the DWI Leibniz-Institut für Interaktive Materialien e.V, Aachen, Germany. The accessible q-range is between 0.011 nm^{-1} and 4.4 nm^{-1} for the SAXS functionality. A Cu source

was used and the detector was the Dectris Pilatus 3 hybrid photon counting detector. A beam wavelength of 1.54 Å was used. The data were reduced by the manufacturer's software/GUI for the instrument, Nano-inXider Version 2.3.2.

- Beamline BL40B2 at SPring-8, Sayo, Japan. The beam energy was 10 keV, while the detector distance was set to 4m, corresponding to a q-range of $0.023\ \text{nm}^{-1} < q < 2.0\ \text{nm}^{-1}$. The temperature was maintained at 25 ^{o}C by a Peletier heating unit. Data treatment for measurements from this beamline were not adjusted for empty capillary readings, as transmission data was difficult to obtain. Thus, only data with clear peaks visible in the spectrum were taken.

- Beamline I22 at the Diamond Light Source, Chilton, United Kingdom. The beamline had an accessible q-range of $0.016\ \text{nm}^{-1} < q < 1.6\ \text{nm}^{-1}$. The data were reduced with standard procedures and masking via the complementary software Data Analysis WorkbeNch (DAWN), with the data further treated by subtracting from the empty cell reading to adjust for the background. Up to 20 samples at a time were loaded into a custom-made capillary holder provided by the beamline. No temperature control units were used, thus the measurements took place at room temperature of approximately 23 °C.

Solubility phase mapping: A solution of NaCMC in non-solvent/water mixture of a known concentration and mixing fraction below the solubility limit was prepared by dissolving NaCMC in said mixture, which was left overnight on a roller mixer to homogenise. Another mixture consisting of the same organic non-solvent and water mixture, which has a mixing fraction between that of the master solution and the estimated solubility limit was also prepared, hereafter referred to as the dilutant. Different ratios of the master solution to the dilutant were added to different clear glass vials (20 mL) and left for approximately an hour to homogenise.

The non-solvent was added drop-wise from a pipette to the vials, until the sample became turbid, judged as the point when a faint blue tinge can be observed against a black background. The overall mass of the sample with the added non-solvent was recorded. Water was added drop-wise to the turbid sample until it became clear again, which will be referred to as the "redissolving point", and the mass was recorded. The concentrations and mixing fractions at the solubility boundary were calculated by taking the

mean of their value at the turbidity point and the redissolving point. The error was taken to be half of the absolute differences in the measured values at these two points.

Estimation of the residual water content: Thermogravimetric analysis (TGA) was carried out to determine the amount of water trapped in the polyelectrolyte solute. 30.144 mg of dialysed and freeze dried NaCMC that had been exposed to air for 24 hours was loaded into a Simultaneous Thermal Analyser (STA) 6000 device (Perkin Elmer). The sample was heated to 120 °C and held at this temperature for 20 minutes, then cooled to approximately 30 °C afterwards. The water content was taken to be the percentage mass loss of the sample at this point, which was estimated to be 18.02%. All plots hereafter are adjusted based on this estimate, with the "real" concentration taken to be (100 - 18.02) % = 81.98 % that of the prepared concentration.

Conductivity and pH measurements: A SevenMulti Dual pH/ conductivity meter (Mettler Toledo) was used for the conductivity measurements. The conductivity probe was inserted into 10 mL polypropylene vials filled with solution, with the temperature sensor fully submerged. Readings were taken when the temperature inside the solution reached that of the water bath. All measurements were carried out at 25^{o}C.

In addition to estimating the ratio of counterion dissociation, conductivity measurements on aqueous NaCMC solutions of various polymer concentrations were carried out to determine the amount of residual salt added by the rheometer. Approximately 5 mL of each solution was prepared, where approximately 2.2-2.3 mL of the solution was extracted and loaded onto the rheometer and a viscometric experiment was carried out for approximately 15 minutes. Conductivity was measured for both the unused and the loaded sample from the rheometer at each concentration, whereby the residual salt concentration can be estimated from the difference in the conductivities.

Rotational rheology: A stress-controlled rheometer (Kinexus-Pro, Netz) with a 1° angle, 40 mm cone-plate, the CP1/40 with 55mm solvent trap geometry was used. The temperature was set to 25°C using a Julabo 1000F heating unit. A solvent trap filled with the same solvent was used for each corresponding sample to mitigate the effect of evaporation, which can be prominent in acetone/water mixtures due to acetone's high vapour pressure. For some measurements with lower concentrations closer to the overlap concentration, the Discovery Hybrid Rheometer (DHR; TA Instruments) was used with a 40mm cone-plate.

Some conductivity measurements were carried out to check for salt im-

parted by the rheometer geometry during measurement. To ensure that sufficient sample was available for conductivity, which was just over 2 mL, a a 2° angle, 60 mm CP2/60: PL65 cone-plate was used.

In general, shear viscosity measurements were carried out for shear rates between 0.1 $s^{-1}$and 1000 s^{-1}. The limiting torque on the Kinexus rheometer is approximately 4 x 10^{-7} Nm; data corresponding to torque values below this limit was trimmed. Moreover, in some cases, there was still a large increase in viscosity at lower shear rates- this is considered an artefact due to instability or evaporation and trimmed.

Rolling ball viscosimetry: The viscosities of NaCMC solutions with added salts (NaCl or NaI) were measured using rolling ball viscosimetry. The rolling ball viscometer offers a higher precision than the rotational rheometers and is thus more suited for the determination of intrinsic viscosities.

NaCMC solutions of various concentrations and ratios of alcohol in the solvent were prepared, with 20 mM added NaI to each sample. The sample viscosities were obtained by measuring the falling time of a steel ball (ball diameter $a = 1.59$ mm) in the capillary (actual diameter $D = 1.6$ mm) held in the LOVIS 2000 ME Microviscometer instrument (Anton-Paar), with the incline of the capillary held at 35 degrees. The error was taken to be the variation coefficient in the viscosity measurement determined by the instrument, with a "floor" value taken to be 0.1%- the default viscosity coefficient for what is considered to be a "stable" reading on the instrument. The measurements were calibrated regularly (approximately once every 15 to 20 measurements) using distilled water.

All the measurements were carried at 35° incline. Only carried out at one angle, or one shear rate for each sample- we ensured that the shear rate corresponds to the Newtonian plateau region by the following approximation Briscoe et al. (1992):

$$\dot{\gamma} = \frac{2V}{D_{cap} - a}$$

Where V is the ball's terminal rolling velocity. Based on a typical run time of around 30 seconds to 5 minutes, we estimate V to be around $\sim 10^{-3} - 10^{-2}$ m s^{-1}, while $D_{cap} - a \sim 10^{-5}$ m, giving a shear rate of approximately $\sim 10^3$ s^{-1} to $\sim 10^2$ s^{-1} closer to the overlap concentration.

3. Results

Light Scattering

We use the refractive index increments at constant chemical potential reported by Brown et alBrown et al. (1964) for NaCMC with DS = 1.06 for wavelengths of $\lambda = 436$ and 546 nm, extrapolated to the wavelengths of our instrument, using the Cauchy equation. Static light scattering data were fitted to the Zimm equation, as shown in the SI. We obtain $M_w \simeq 360$ kg/mol, $R_g \simeq 72$ nm and $A_2 = 2.4 \times 10^{-3}$ mLg^2/mol. The molar mass corresponds to a weight averaged degree of polymerisation of $N \simeq 1500$.

Dynamic light scattering correlation functions were fitted to a cumulant expansion to obtain the inverse decay time (Γ) as a function of the scattering wave-vector q. The diffusion coefficient of the chains was obtained using:

$$\Gamma/q^2 = D(1 + k_D c)(1 + Cq^2 R_g^2)$$

where D the translational diffusion coefficient of the chains, k_D the diffusion second virial coefficient and C is a constant that depends on the shape and polydispersity of the macromolecule.Schmidt (1984)

The hydrodynamic radius (R_H) was calculated from the Stokes-Einstein equation to be: 31 nm. k_D and C were measured to be 460 cm^3/g and 0.13 respectively.

Phase Mapping

The non-solvent content at the phase boundary is plotted as a function of polymer concentration in fig. 1 for the three non-solvents studied. The critical mole fraction of non-solvent at the phase boundary is seen to decrease with increasing polymer concentration. For the other experiments performed, master solutions of no more than 50 wt.% non-solvent were prepared to keep the samples in the soluble region.

Small-Angle X-ray Scattering

For polyelectrolytes in salt-free solution, there is a peak in the total structure factor, at wave-vector $q = q^*$,which can be related to the correlation length ξ as:Nierlich et al. (1979, 1985); Combet et al. (2012); Lopez et al. (2015, 2018)

$$\xi = \frac{2\pi}{q^*}$$

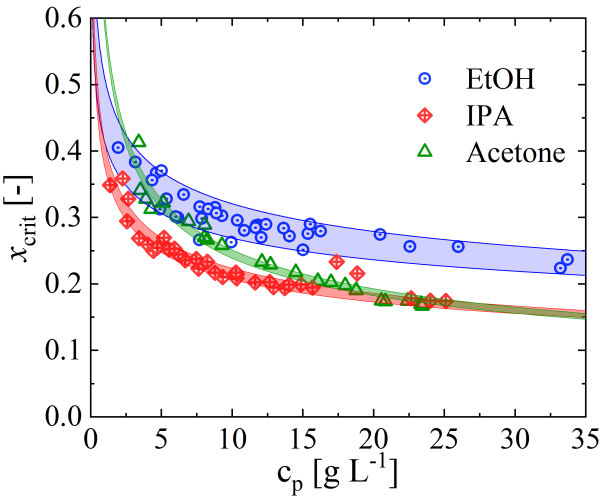

Figure 1: The solubility phase map of NaCMC in ethanol-water (blue), isopropanol-water (red) and acetone-water (green) mixtures. The lines represent the estimated boundary separating the soluble and the insoluble regions. x_{crit} represents the critical mole fraction of the non-solvent in solution at the solubility boundary.

The reduced data for SAXS were trimmed visually, to leave only the local peak corresponding to the correlation length, as shown in fig. 2. The logarithmic values of the intensity and scattering wavenumber q were fit to a fourth-order polynomial, from which the maximum is taken to be the peak. The value of q_{max} is the position corresponding to the peak.

Conductivity

The conductivity of NaCMC in aqueous solutions with different mass fractions of ethanol was recorded as a function of polymer concentration. The results of these measurements are summarised in the table of results in the supplementary information.

Determination of the intrinsic viscosity

The viscosities of the NaCMC solutions in excess salt were measured via rolling ball viscosimetry for NaCMC in aqueous solutions with 0.01 M, 0.1 M and 0.2 M added NaCl. In addition, measurements for NaCMC in water/ethanol mixtures with 0.02 M added NaI salt was measured, the details of which are included in the SI. Sodium Iodide was chose for these experiments due to it's greater solubility in ethanol compared to NaCl.

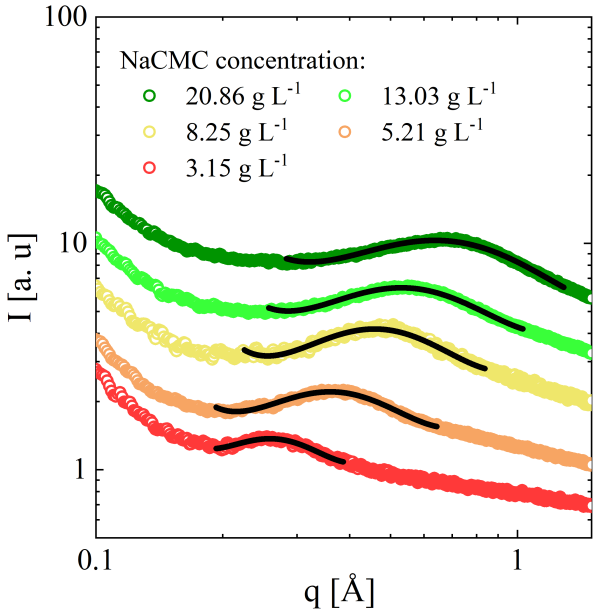

Figure 2: The SAXS spectra of NaCMC solutions of different NaCMC concentrations in 20 wt% ethanol, with intensity in arbitary units. The black lines were added to illustrate the 4th order polynomial fit in the vicinity of the peak, which is chosen visually. The peak position is taken to be the q value corresponding to the maximum of the peak region.

The reduced viscosity ($\eta_{red} = \eta_{sp}/c$) and inherent viscosity ($\eta_{inh} = ln(\eta_{rel})/c$) were plotted against the concentration and fit with the Huggins and Kraemer's equations:Huggins (1942); Kraemer (1938); Gosteva et al. (2023)The solvent viscosities were taken from 36

$$\frac{\eta_{sp}}{c} = [\eta] + k_H[\eta]^2 c \tag{1}$$

$$\frac{ln(\eta_{rel})}{c} = [\eta] + k_K[\eta]^2 c \tag{2}$$

With $[\eta]$ being the intrinsic viscosity i.e. reduced viscosity in the zero-concentration limit, k_H being the Huggins constant, k_K the Kraemer's constant and $\eta_{rel} = \eta_{sp} - 1$ the relative viscosity. Data for the intrinsic viscosity as a function of ethanol content are provided in the supporting information.

An example of the Huggins and Kraemer's plot for the determination of the intrinsic viscosities in aqueous solution with different added salt concentration is shown in figure 3. Both methods are seen to yield similar results

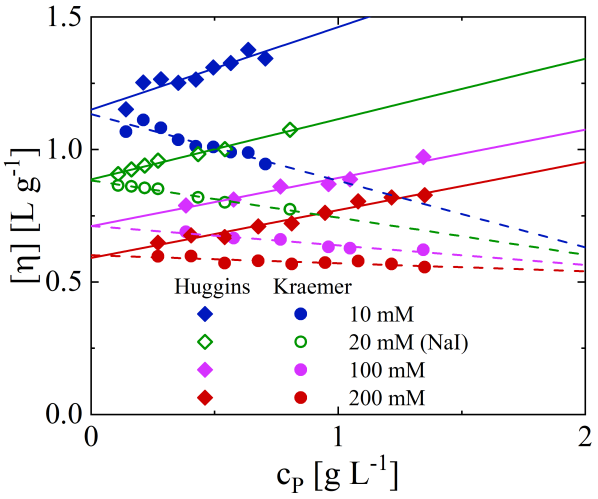

Figure 3: Reduced viscosity plotted against the concentration for NaCMC solutions with added NaCl (0.01, 0.1 and 0.2 M) and with added NaI (0.02 M). The solid and dashed lines represent fits to 1 and 2 respectively.

for the intrinsic viscosity of the samples. The intrinsic viscosities reported below are calculated by taking an average of the values obtained from the two methods.

Rheology

The viscosity data, measured a function of shear rate were fit to the Carreau-Yasuda model:Yasuda et al. (1981)

$$\eta(\dot{\gamma}) = \frac{\eta_0}{[1 + (\tau\dot{\gamma})^a]^{n/a}} \tag{3}$$

where η_0 is the zero-shear viscosity, τ the longest relaxation time of the systems, n the flow index and a a fit-parameter that sets the broadness of the transition between the Newtonian and power-law regime. The specific viscosity for a given polymer concentration was extracted along with the error calculated from the fitting covariance, with the solvent viscosity η_s for different solvent mixture obtained from the literature.Khattab et al. (2012); Howard and McAllister (1958); Cygler and Freeman (1984) Examples are given in part (a) of figure 4 for NaCMC solutions in 30/70 EtOH/water by weight. Values for the extracted parameters are listed in the supporting information.

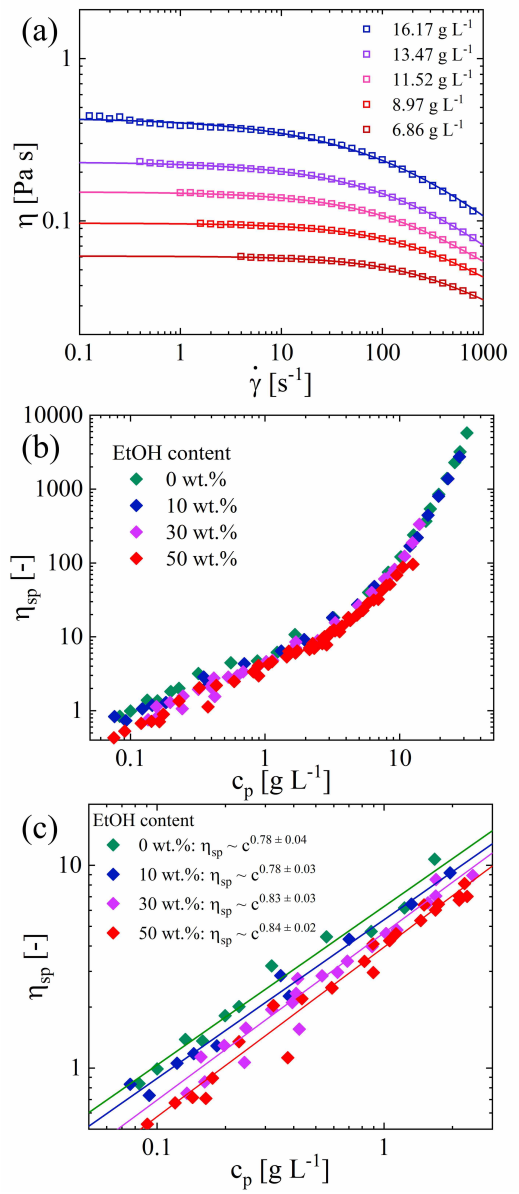

Figure 4: The zero-shear viscosity is extracted by fitting the Carreau-Yasuda model (Eq. 3) to the viscosity vs. shear rate (a) shows some of the curves for samples with 30 wt.% ethanol content at different polymer concentrations (b) is the viscosity vs. concentration plot of several different NaCMC in ethanol-water sample sets (c) a zoomed in view of the viscosity-concentration plot. A straight line is fit to the log-log plot to extract a scaling exponent and the overlap concentration.

The specific viscosities of NaCMC solutions in different aqueous ethanol mixtures are plotted as a function of concentration in figure 4b. The data are fitted to the following cross-over function:

$$\eta_{sp}(c) = \left(\frac{c}{c^*}\right)^{\alpha}\left[1 + \left(\frac{c}{c_e}\right)^{\beta}\right] \tag{4}$$

where c^* is the overlap concentration, α is the non-entangled viscosity-concentration exponent, c_e is the entanglement concentration and $\alpha + \beta$ is the entangled viscosity-concentration exponent.Lopez (2019)

Examples of the fit to Eq. 4 are provided in the supporting information. Fits to the non-entangled region for solutions with various ethanol content are shown in figure 4c. The best-fit values of α are indicated on the legend. The best-fit parameters obtained by applying Eq. 4 to solutions in the various mixed solvent studied are tabulated in the supporting information. The dynamics for $c > c_e$ will be discussed in a separate manuscript, here we focus on the semidilute non-entangled viscosities only, from which it is easier to extract conformational information.

4. Discussion

Table 2 lists the intrinsic viscosity and the Huggins and Kraemer coefficients of the NaCMC polymer in aqueous solutions with different concentrations of added salt. As expected, the intrinsic viscosity decreases and the Huggins coefficient increases with increasing c_S. Using the Mark-Howink-Sakurada relationships from ref 48, the degree of polymerisation is estimated to be $N \simeq 1200$, from the $[\eta]$ value in 0.01 M and $N \simeq 1500$ from the $[\eta]$ value in 0.1 M. These agree reasonably well with the estimate from light scattering. In the following calculations we use the light scattering estimate for N as this is our most direct estimate.

c_S [M]	$[\eta]$ [L g^{-1}]	k_H [-]	k_K [-]
0.01	1.133 ± 0.017	0.24 ± 0.08	-0.20 ± 0.06
0.02[a]	0.883 ± 0.004	0.29 ± 0.03	-0.18 ± 0.02
0.1	0.712 ± 0.010	0.36 ± 0.08	-0.08 ± 0.04
0.2	0.601 ± 0.007	0.52 ± 0.08	-0.16 ± 0.04

Table 1: Intrinsic viscosity and associated parameters for NaCMC in excess salt solutions. [a] added salt is NaI, for all other samples, it is NaCl.

4.1. Phase behaviour

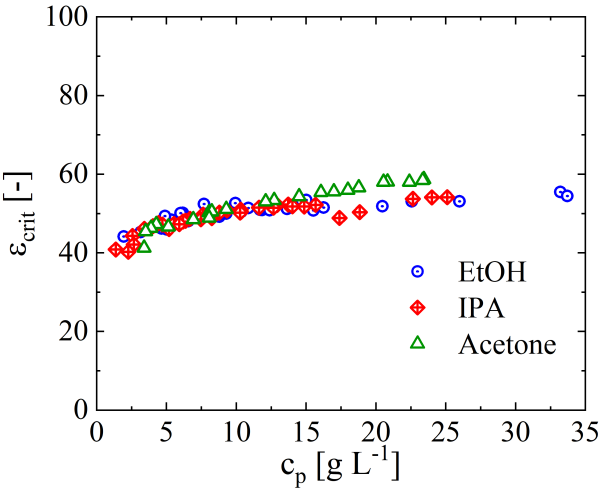

Figure 5: Dielectric constant of water/non-solvent mixture at precipitation boundary (ϵ_{crit}, see figure 1) as a function of polymer concentration. Colours have the same meaning as in Figure 1.

The phase boundary data in figure 1 were used to calculate the dielectric constant at the phase boundary for the three aqueous/non-solvent systems studied. The dielectric constant at x_{crit} is plotted as a function of polymer concentration in Fig. 5. The dielectric constants were estimated by taking the mass fraction weighted sum of the two constituents in the solvent mixtures, see the SI for details. The results in figure 5 show that for a given polymer concentration, the dielectric constant near the phase boundary is approximately the same for the three non-solvents studied.

4.2. SAXS

Figure 6a plots the correlation length of NaCMC as a function of polymer concentration in mixtures of water and ethanol with different ethanol mass fraction. All the data are seen to follow a power-law of $\xi \sim c^{-1/2}$. The scaling model of de Gennes and co-workers predicts $\xi \propto c^{-\nu/(3\nu-1)}$, where ν is the solvent quality exponent, which relates the end-to-end distance of a chain in dilute solution R to it's degree of polymerisation by $R \propto N^{\nu}$. The observed dependence therefore corresponds to $\nu = 1$, in agreement with earlier estimates based on the N dependence of c^* of NaCMC in DI water.Lopez

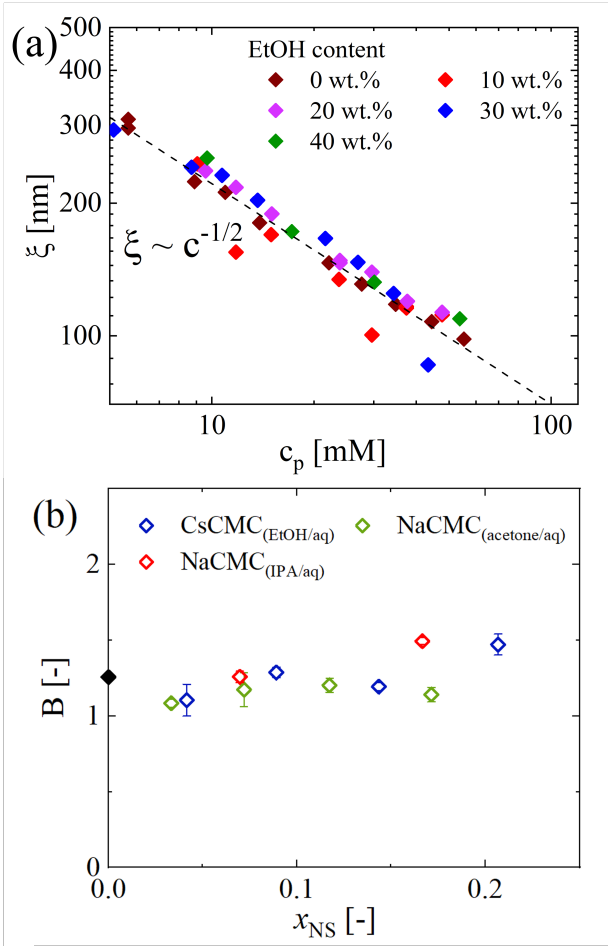

Figure 6: a: Correlation length of CsCMC and NaCMC solutions in different mixtures of ethanol and water as a function of concentration of polyelectrolytes in molar. The line shows a power-law with exponent -1/2, as predicted by the scaling model. b: chain stretch parameter B against the non-solvent (EtOH) mass fraction x_{NS}.

(2020) Similar behaviour was observed for solutions in mixtures of 2-propanol and water and acetone and water. The data for these are presented in the supporting information.

The scaling model of Dobrynin et alDobrynin et al. (1995) predicts the correlation length of semidilute solutions in salt-free solvents to be:

$$\xi = \sqrt{\frac{B}{bc}} \tag{5}$$

where B is the chain stretch parameter which describes the local folding of polyelectrolyte chains in solution: $B = 1$ corresponds to a fully stretched chain and values of $B > 1$ correspond to increased local folding. b is the chemical monomer length and c the concentration in number of chemical monomers per unit volume.

The chain stretch parameter, calculated from the correlation length data in ethanol/water, 2-propanol/water and acetone/water mixtures is plotted as a function of non-solvent fraction in figure 6b, where B is seen to be insensitive to the presence of the non-solvent content, taking a fixed value of $B \simeq 1.4$. This is $\simeq 20\%$ larger larger than the value estimated for aqueous solutions from [47] for DS = 1. We discuss the independence of B on x_{NS} in more detail below, following the discussion of counterion condensation.

4.3. Conductivity

The model of Colby et al. was used to estimate the fraction of monomers with a dissociated counterion (f) from conductivity data.Colby et al. (1997); Bordi et al. (2004) The model calculates the specific conductance Λ of a salt-free polyelectrolyte solution:

$$\Lambda = \left(\lambda_c + \frac{cf\xi^2 e^2 \ln(\xi/D)}{3\pi\eta_s}\right) f \tag{6}$$

where $\lambda_c \equiv e\mu_c$ is the specific conductance of the counterion, with e being the electron charge and μ_c the counterion mobility, f is the fraction of monomers bearing a dissociated counterion, η_s is the solvent viscosity and D is the chain's cross-sectional diameter, taken to be 1.2 Å.Lopez et al. (2015)

Values for f, calculated from conductivity data using equation 6, are plotted as a function of concentration for different ethanol mass fractions in figure 7a. The fraction of charged monomers is seen to be a weakly increasing function of concentration over the range studied. Note that all the data in figure 7 corresponds to the semidilute regime. The fraction of monomers bearing a dissociated charge (f) is related to the fraction of dissociated counterions (f') as $f' = DSf$. In water, the value of $f' \simeq 0.495$ is slightly higher than the values of $f' \simeq 0.4 - 0.43$ reported by Ray et alRay et al. (2016) for NaCMC with DS = 0.9-1.2 at 35 °C. The discrepancy likely arises in part from the

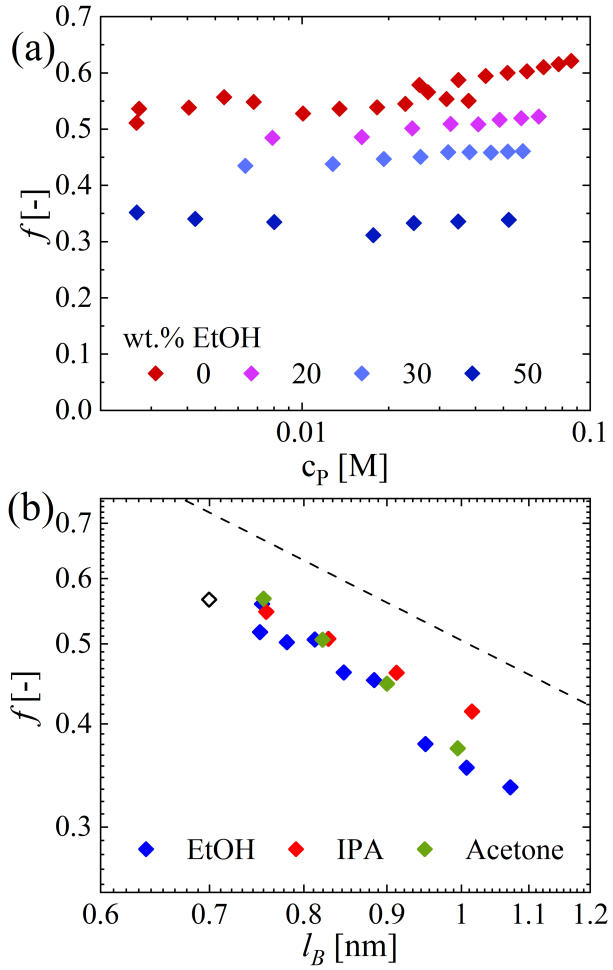

Figure 7: a: fraction of monomers with a dissociated counterion f for each NaCMC/ethanol/water system at different concentrations b: f as a function of the Bjerrum length of the solvent media for water/ethanol (black circles) and water/IPA (blue diamonds). The dashed line is the prediction of the Manning model.

fact that we use experimentally measured values for the correlation length, while Ray et al calculate ξ for their systems using Dobrynin et al'sDobrynin et al. (1995) scaling model.

The value of f averaged over the different NaCMC concentrations studied for a given non-solvent mass fraction is plotted as a function of the Bjerrum length of the solvent media in figure 7b. The values of f are, within ex-

perimental error, a function of the Bjerrum length of the mixed solvent, independent of the non-solvent used. The Manning prediction ($f = b/l_B$) is shown as a dashed line. This captures the observed experimental trend but is $\simeq \times 1.3$ too high. The disagreement is not surprising as Manning's model was derived for stiff polyelectrolytes in dilute solution, and here we consider only semidilute solution data.

4.3.1. Determination of residual salt of rheology samples.

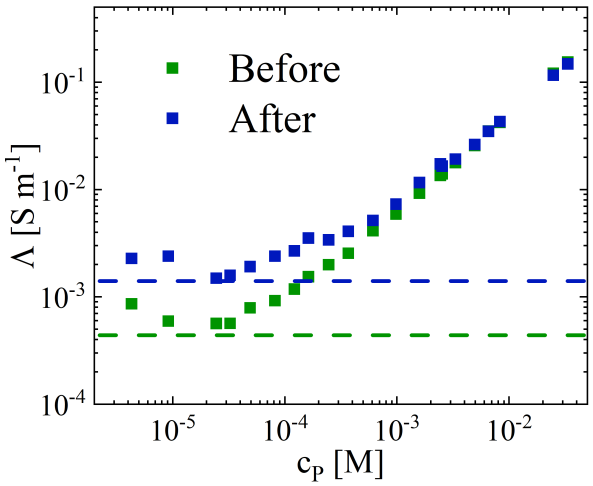

Figure 8: Conductivity as a function of NaCMC concentrations for samples before (green symbols) and after (blue symbols) being measured in the rheometer. Dashed lines indicate ρ_0, the conductivity values measured for the pure solvent with and without being measured on the Kinexus rheometer.

Solvent	Conductivity before [10^{-4} S m^{-1}]	Conductivity after [10^{-4} S m^{-1}]
Ethanol	0.775	1.04
2-Propanol	0.048	0.099
Acetone	0.587	3.07

Table 2: Intrinsic viscosity and associated parameters for NaCMC in excess salt solutions. [a] added salt is NaI, for all other samples, it is NaCl.

Han et al. recently reported conductivity data for sodium polystyrene sulfonate over a very broad concentration range.Han et al. (2022) At low polymer concentrations, the conductivity of their solutions was found to be

independent of NaPSS concentration at a value of $\rho_0 \simeq 5 - 8 \times 10^{-3}$ S m^{-1}. According to their estimate, this corresponds to a residual salt concentration of $c_{S,res} \simeq 2 \times 10^{-4}$ M, and is higher than the residual salt concentration of water exposed to air, suggesting that contact with the rheometer's measuring geometry may increase the residual salt of the samples. In order to check whether this is also the case for our samples, we measured the conductivity of NaCMC solutions before and after measuring them on the Kinexus rheometer. We used the 60 mm plate geometry for these experiments, as it was easier to extract sufficient samples for the conductivity measurement at once, whereas the 40 mm plates require multiple extractions.

The results are plotted in figure 8. At high concentrations, the conductivity of the samples is seen to be nearly identical. At low concentrations, the samples after measurements consistently exhibit higher solution conductivities than those which have not been measured on the rheometer. The difference in conductivity between these samples is $\simeq 10^{-3}$ S m^{-1}. Assuming a specific ionic conductivity of 130 S cm^2 mol^{-1}, this corresponds to a residual salt concentration of $\simeq 6 \times 10^{-5}$ M.Robinson and Stokes (2002) This same difference is observed for DI water before and after it is measured on the Kinexus 60mm geometry. The increase the conductivity of DI water after a measurement in the 40 mm cone-plate DHR rheometer gave a similar increase. The results therefore clearly show that the rheology measurement introduces an additional residual salt on the samples. The reason why this contamination occurs is not clear to us.

The pH of the samples before and after being measured in the Kinexus rheometer was also recorded. There is a small but noticeable decrease in the pH for the samples removed from the rheometer, as shown in figure 9. Based on the relation of pOH = 14 - pH = -$log[OH^-]$, the net hydroxide ion concentration difference as a result of rheometer contamination was calculated to be between 10^{-7} M to 10^{-5} M in the range of concentrations measured.

4.4. Solution viscosity

4.4.1. Overlap concentration in mixed solvents

The scaling theory predicts for the overlap concentration of polyelectrolyte solutions:

$$c^* = \left(\frac{B^3}{b^3 N^2}\right)\left[1 + \frac{2c_S}{fc^*}\right]^{-1.5} \tag{7}$$

The term in round brackets corresponds to the scaling prediction for salt-free solutions and the term in square brackets corresponds to the effect of

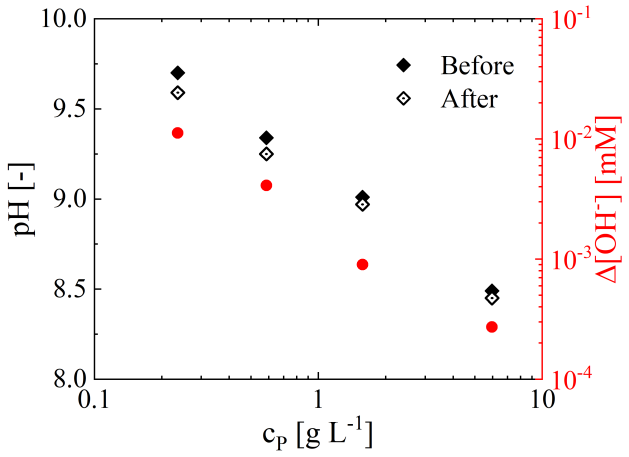

Figure 9: pH as a function of NaCMC concentration for samples before and after being measured in the rheometer. Red points are the estimated change in OH^- concentration.

low molecular weight salts in the solution. For solutions in water, we find $c^* \simeq 0.5$ mM. Using the residual salt value of $c_S = 6 \times 10^{-5}$ M, the overlap concentration in salt-free water can be estimated to be $c^* \simeq 0.37$ mM.

The values of the overlap concentration are plotted as a function of the non-sovlent mass fraction for water/ethanol, water/acetone and water/IPA mixtures in figure 10a. The corresponding values of the stretching parameter B calculated from Eq. 7 with $c_S = 0$ are plotted on part b. If $c_S = 6 \times 10^{-5}$ M is used instead, B decreases by $\simeq 10\%$. The near-independence of B on non-solvent mass fraction agrees with the SAXS results within experimental error. The viscosimetric estimates for B are significantly larger than the more direct measurements by SAXS. Similar differences have been reported for NaCMC and other systems in earlier studies.Lopez et al. (2015, 2018); Di Cola et al. (2004)

The overlap concentration of NaCMC in 0.02 M NaI added salt as a function of ethanol mass fraction is presented in the supporting information. As for the salt-free case, c^* weakly increases with x_{NS}.

4.4.2. Semidilute non-entangled viscosity scaling

In the semi-dilute, non-entangled concentration regime, the specific viscosity scaling is:

$$\eta_{sp} \simeq \frac{N}{c\xi^3} \sim c^{\frac{1}{3\nu-1}} \tag{8}$$

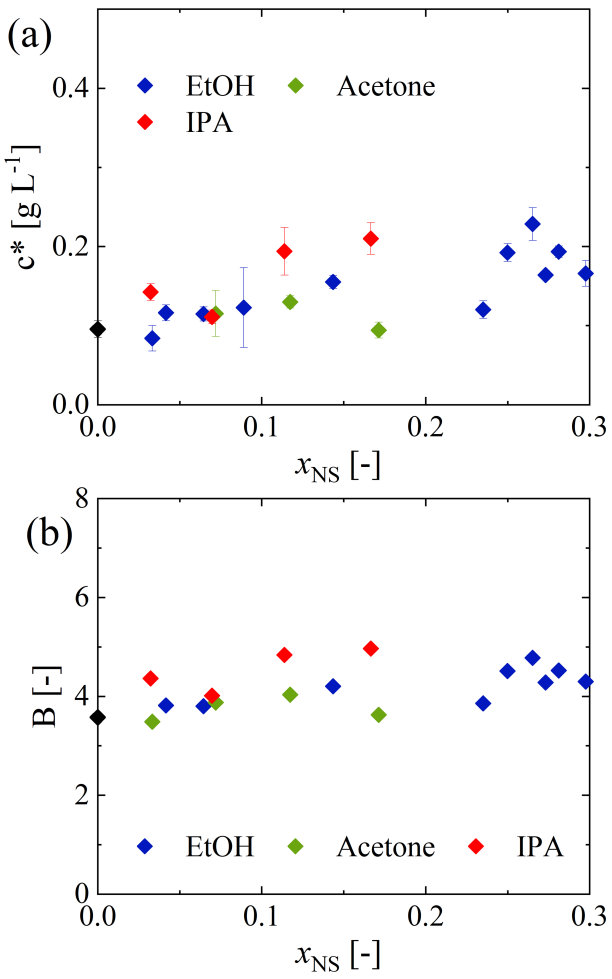

Figure 10: (a) The c^* at different mixing ratios and (b) the stretch parameter B of the chains at the corresponding mixing ratios, calculated from the equation $B = b(c^* N^2)^{\frac{1}{3}}$.

where ν is the solvent quality exponent, which determines the relationship between the end-to-end distance of a correlation blob and the number of monomers in it. For salt-free solutions, $\xi \propto c^{-1/2}$ and $\eta_{sp} \propto c^{1/2}$ is predicted. As discussed, the correlation length scaling agrees well with the experimental results in the various solvent media studied. By contrast, the specific viscosity shows stronger exponents which are not anticipated theoretically.

The scaling theory expects the specific viscosity of semidilute non-entangled solutions to be:

$$\eta_{sp} = \frac{c^{1/2}}{B^{2/2}}\Big[1 + \frac{2c_S}{fc}\Big]^{-0.75} \tag{9}$$

In the high added salt limit ($2c_S \gg fc$, Eq. 9 predicts $\eta_{sp} \propto c^{5/4}$, in agreement with experimental observations.Gulati et al. (2023); Lopez et al. (2017); Boris and Colby (1998) For salt-free conditions, Eq. 9 expects $\eta_{sp} \propto c^{1/2}$ (the Fuoss law). These values correspond to Eq. 8 for the $\nu = 0.59$ and $\nu = 1$ cases. The Fuoss limit is observed for some systems Lopez and Richtering (2018); Gulati et al. (2023); Lopez et al. (2021). However, many studies have reported higher $\eta_{sp} - c$ exponents.Lopez et al. (2017); Kujawa et al. (2006, 2004); Behra et al. (2019); Lopez (2019, 2020); Lopez and Richtering (2019a); Matsumoto et al. (2022); Han and Colby (2021); Lopez and Richtering (2019b) The most commonly suggested explanation for this observation is to assume the presence of residual salts in the samples.Dobrynin and Jacobs (2021); Jacobs et al. (2021); Chen et al. (2021) For $2c_S \sim fc$ values, the $\eta_{sp} - c$ curve displays a broad cross-over between $\eta_{sp} \sim c^{5/4}$ ($\nu = 0.59$) at low polymer concentrations to $\eta_{sp} \sim c^{1/2}$ at high c ($\nu = 1$). This can result in apparent values of the ν exponent in between those limits.

Figure 11 plots the exponent ν extracted from fitting semidilute unentangled viscosity data to eq. 8. The values of the solvent quality exponent take a constant value of $\nu \simeq 0.75$ independent of non-solvent weight fraction and non-solvent type. In the supporting information, we repeat this plot for selected non-solvent contents, but instead of fitting η_{sp} vs. c, we fit $\eta_{sp}/[1 + \frac{2c_S}{fc}]^{-3/4}$, with $c_S = 6 \times 10^{-5}$ M determined from the conductivity measurements. These viscosity values should correspond to the true salt-free case. The values of ν increase slightly ($\simeq 10\%$) relative to the case where no residual salt correction is applied, but still do not match the scaling prediction of $\nu = 1$ for salt-free solutions.

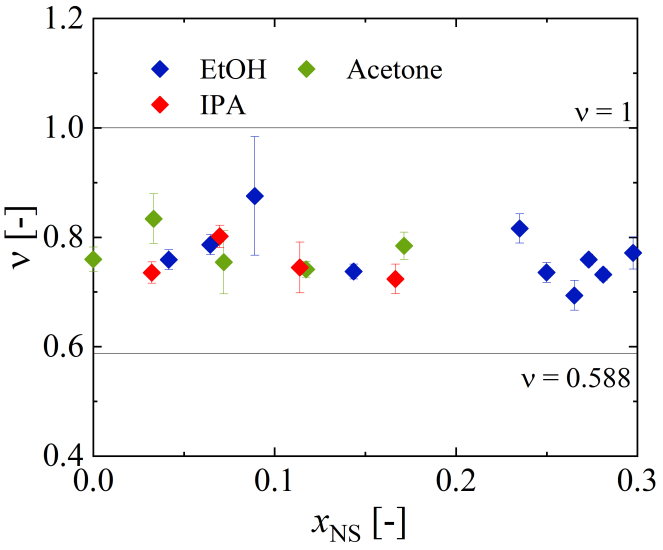

Figure 11: Plot of the Flory exponent for NaCMC solution in different organic-water mixtures of varying mole fractions of the non-aqueous component against the non-solvent molar fraction in the solvent mixture, x_{NS}. The lines denote the good solvent ($\nu = 0.588$) and salt-free polyelectrolyte ($\nu = 1$) limits.

4.5. Conformation of CMC chain in mixed solvents

The parameter B is predicted by the theory of Dobrynin et al to correspond to the ratio of the contour length of an electrostatic blob relative to its end-to-end distance. The electrostatic blob is the lengthscale at which electrostatic interactions along a section of the chain are of the order of the thermal energy k_BT and is therefore expected to correspond to the Bjerrum length (l_B) when there is more than one dissociated charge per Kuhn segment. For NaCMC, the bare (intrinsic) Kuhn segment has been estimated as $l_{K,0} \simeq$ 10 nm (20 monomers), which, based on the conductivity results is expected to have $\simeq$ 10 dissociated charges in water and $\simeq$ 6 dissociated charges at the highest non-solvent fractions studied. Therefore, $l_{K,0} > \xi_{el} \simeq l_B$ is expected to hold over the entire non-solvent composition range studied.

Inside the correlation blob, the chain conformation is expected to be like that in dilute solution. Chains remain rigid on lengthscales of up to $\simeq$ 10 nm due to the intrinsic (non-electrostatic) rigidity of the backbone, as quantified by the Kuhn length. On larger distances, a rigid-like conformation is maintained due to strong electrostatic stretching, predicted by the scal-

ing model on lengthscales larger than the electrostatic blob.Dobrynin et al. (1995); Lopez et al. (2015) Varying the non-solvent content decreases the effective charge of the backbone, but since there are always several dissociated charges per Kuhn segment, the $l_{K,0} > \xi_{el}$ relationship continues to hold and a rigid-like conformation is maintained on all lengthscales smaller than the correlation length. Our finding that the stretch parameter is independent of the effective charge fraction over the range of conditions studied is therefore consistent with the scaling model of Dobrynin et al.

5. Summary and conclusions

Solutions of carboxymethyl cellulose in mixtures of water and polar non-solvents were studied using small-angle X-ray and rheological techniques. The viscometric profile and correlation length plots obtained from SAXS measurements show minor differences in solutions of NaCMC in several different water-polar liquid mixtures. These results imply that although the dielectric constant and solvent quality of the medium decreases, the chain conformation is unchanged, so long as the polyelectrolyte remains soluble in solution.

On the other hand, conductivity measurements demonstrated an increase in the ratio of counterions dissociating from the polymer chains as non-solvent ratio increases. Due to water having a higher dielectric constant than the added non-solvents, this is qualitatively consistent with the prediction by Manning theory for dilute solutions. However, the power law between the fraction of condensed counterions and the Bjerrum length are stronger than the Manning theory prediction.

The independence of polymer conformation on the degree of dissociated counterions is consistent with the scaling theory of Dorbynin et al as the bare Kuhn length ($\simeq 10$ nm) is larger than the electrostatic blob size ($\xi_T \simeq l_B \simeq 1$ nm).

Acknowledgements

We greatly appreciate the assistance of Lars Voleske for carrying out and helping with the phase mapping and conductivity experiments. We thank Dr. Noboru Ohta (SPring-8) for technical assistance with experiments outlined in project proposal 56901 at the BL40B2 beamline. We express our gratitude to Dr. Martin Dulle (Forschungszentrum Jülich) and Dr. Max

Hohenschutz (RWTH) for their help with measurements on the "Ganesha-Air" SAXS system and the subsequent data analysis and fo performing the titration experiments to determine the DS of the polymer. In addition, the authors would like to thank Diamond Light Source for beamtime (proposal SM-33596), and Dr. Thomas Zinn, Dr. Michal and the staff of beamline I22 for assistance with sample preparation, small-angle X-ray scattering measurements and data extraction from AP33. This work was supported by the DFG project RI 560/26-1.

References

Arancibia, C., Navarro-Lisboa, R., Zúñiga, R., Matiacevich, S., et al., 2016. Application of cmc as thickener on nanoemulsions based on olive oil: Physical properties and stability. International Journal of Polymer Science 2016.

Bajul, A., Gerbaud, V., Teychene, S., Devatine, A., Bajul, G., 2017. Effect of carboxymethylcellulose on potassium bitartrate crystallization on model solution and white wine. Journal of Crystal Growth 472, 54–63.

Behra, J.S., Mattsson, J., Cayre, O.J., Robles, E.S., Tang, H., Hunter, T.N., 2019. Characterization of sodium carboxymethyl cellulose aqueous solutions to support complex product formulation: A rheology and light scattering study. ACS Applied Polymer Materials 1, 344–358.

Böhm, N., Kulicke, W.M., 1997. Optimization of the use of polyelectrolytes for dewatering industrial sludges of various origins. Colloid and Polymer Science 275, 73–81.

Bordi, F., Cametti, C., Colby, R., 2004. Dielectric spectroscopy and conductivity of polyelectrolyte solutions. Journal of Physics: Condensed Matter 16, R1423.

Boris, D.C., Colby, R.H., 1998. Rheology of sulfonated polystyrene solutions. Macromolecules 31, 5746–5755.

Briscoe, B., Luckham, P., Ren, S., 1992. An assessment of a rolling-ball viscometer for studying non-newtonian fluids. Colloids and surfaces 62, 153–162.

Brown, W., Henley, D., Ohman, J., 1964. Sodium carboxymethyl cellulose experimental study of influence of molecular weight and ionic strength on polyelectrolyte configuration. Arkiv Kemi 22, 189–206.

Buscall, R., Corner, T., 1982. The phase-separation behaviour of aqueous solutions of polyacrylic acid and its partial sodium salts in the presence of sodium chloride. European Polymer Journal 18, 967–974.

Chen, G., Perazzo, A., Stone, H.A., 2021. Electrostatics, conformation, and rheology of unentangled semidilute polyelectrolyte solutions. Journal of Rheology 65, 507–526.

Colby, R.H., Boris, D.C., Krause, W.E., Tan, J.S., 1997. Polyelectrolyte conductivity. Journal of Polymer Science Part B: Polymer Physics 35, 2951–2960.

Combet, J., Lorchat, P., Rawiso, M., 2012. Salt-free aqueous solutions of polyelectrolytes: Small angle x-ray and neutron scattering characterization. The European Physical Journal Special Topics 213, 243–265.

Cygler, J., Freeman, G.R., 1984. Effects of solvent structure on electron reactivity and radiolysis yields: 2-propanol/water mixed solvents. Canadian journal of chemistry 62, 1265–1270.

Dakhara, S., Anajwala, C., 2010. Polyelectrolyte complex: A pharmaceutical review. Systematic Reviews in Pharmacy 1.

DeButts, E., Hudy, J., Elliott, J., 1957. Rheology of sodium carboxymethylcellulose solutions. Industrial & Engineering Chemistry 49, 94–98.

Di Cola, E., Plucktaveesak, N., Waigh, T., Colby, R., Tan, J., Pyckhout-Hintzen, W., Heenan, R., 2004. Structure and dynamics in aqueous solutions of amphiphilic sodium maleate-containing alternating copolymers. Macromolecules 37, 8457–8465.

Dobrynin, A.V., Colby, R.H., Rubinstein, M., 1995. Scaling theory of polyelectrolyte solutions. Macromolecules 28, 1859–1871.

Dobrynin, A.V., Jacobs, M., 2021. When do polyelectrolytes entangle? Macromolecules 54, 1859–1869.

Dobrynin, A.V., Rubinstein, M., 2005. Theory of polyelectrolytes in solutions and at surfaces. Progress in Polymer Science 30, 1049–1118.

Dürig, G., Banderet, A., 1950. Sur la structure des solutions aqueuses de carboxymethylcellulose. Helvetica Chimica Acta 33, 1106–1118.

Eisenberg, H., Casassa, E.F., 1960. Aqueous solutions of salts of poly (vinylsulfonic acid). Journal of Polymer Science 47, 29–44.

Eisenberg, H., Mohan, G.R., 1959. Aqueous solutions of polyvinylsulfonic acid: Phase separation and specific. interactions with ions, viscosity, conductance and potentiometry. The Journal of Physical Chemistry 63, 671–680.

Eisenberg, H., Woodside, D., 1962. Multicomponent polyelectrolyte solutions. part ii. excluded volume study of polyvinylsulfonate alkali halide systems. The Journal of Chemical Physics 36, 1844–1854.

Elliot, J.H., Ganz, A., 1974. Some rheological properties of sodium carboxymethylcellulose solutions and gels. Rheologica Acta 13, 670–674.

Feddersen, R.L., Thorp, S.N., 1993. Sodium carboxymethylcellulose, in: Industrial gums. Elsevier, pp. 537–578.

Gosteva, A., Gubarev, A.S., Dommes, O., Okatova, O., Pavlov, G.M., 2023. New facet in viscometry of charged associating polymer systems in dilute solutions. Polymers 15, 961.

Gulati, A., Jacobs, M., Lopez, C.G., Dobrynin, A.V., 2023. Salt effect on the viscosity of semidilute polyelectrolyte solutions: Sodium polystyrenesulfonate. Macromolecules 56, 2183–2193.

Han, A., Colby, R.H., 2021. Rheology of entangled polyelectrolyte solutions. Macromolecules 54, 1375–1387.

Han, A., Uppala, V.V.S., Parisi, D., George, C., Dixon, B.J., Ayala, C.D., Li, X., Madsen, L.A., Colby, R.H., 2022. Determining the molecular weight of polyelectrolytes using the rouse scaling theory for salt-free semidilute unentangled solutions. Macromolecules 55, 7148–7160.

Hollabaugh, C., Burt, L.H., Walsh, A.P., 1945. Carboxymethylcellulose. uses and applications. Industrial & Engineering Chemistry 37, 943–947.

Howard, K.S., McAllister, R.A., 1958. The viscosity of acetone-water solutions up to their normal boiling points. AIChE Journal 4, 362–366.

Huggins, M.L., 1942. The viscosity of dilute solutions of long-chain molecules. iv. dependence on concentration. Journal of the American Chemical Society 64, 2716–2718.

Jacobs, M., Lopez, C.G., Dobrynin, A.V., 2021. Quantifying the effect of multivalent ions in polyelectrolyte solutions. Macromolecules 54, 9577–9586.

Jimenez, L.N., Martinez Narvaez, C.D., Sharma, V., 2020. Capillary breakup and extensional rheology response of food thickener cellulose gum (nacmc) in salt-free and excess salt solutions. Physics of Fluids 32, 012113.

Jimenez, L.N., Martinez Narvaaez, C.D., Sharma, V., 2022. Solvent properties influence the rheology and pinching dynamics of polyelectrolyte solutions: Thickening the pot with glycerol and cellulose gum. Macromolecules 55, 8117–8132.

Kestin, J., Khalifa, H.E., Correia, R.J., 1981. Tables of the dynamic and kinematic viscosity of aqueous nacl solutions in the temperature range 20–150 c and the pressure range 0.1–35 mpa. Journal of physical and chemical reference data 10, 71–88.

Khattab, I.S., Bandarkar, F., Fakhree, M.A.A., Jouyban, A., 2012. Density, viscosity, and surface tension of water+ ethanol mixtures from 293 to 323k. Korean Journal of Chemical Engineering 29, 812–817.

Komorowska, P., Różańska, S., Różański, J., 2017. Effect of the degree of substitution on the rheology of sodium carboxymethylcellulose solutions in propylene glycol/water mixtures. Cellulose 24, 4151–4162.

Kraemer, E.O., 1938. Molecular weights of celluloses and cellulose derivates. Industrial & Engineering Chemistry 30, 1200–1203.

Kujawa, P., Audibert-Hayet, A., Selb, J., Candau, F., 2004. Rheological properties of multisticker associative polyelectrolytes in semidilute aqueous solutions. Journal of Polymer Science Part B: Polymer Physics 42, 1640–1655.

Kujawa, P., Audibert-Hayet, A., Selb, J., Candau, F., 2006. Effect of ionic strength on the rheological properties of multisticker associative polyelectrolytes. Macromolecules 39, 384–392.

Lankalapalli, S., Kolapalli, V., 2009. Polyelectrolyte complexes: A review of their applicability in drug delivery technology. Indian journal of pharmaceutical sciences 71, 481.

Lochhead, R., et al., 2017. The use of polymers in cosmetic products. Cosmetic science and technology 13, 171–221.

Loh, P., Deen, G.R., Vollmer, D., Fischer, K., Schmidt, M., Kundagrami, A., Muthukumar, M., 2008. Collapse of linear polyelectrolyte chains in a poor solvent: when does a collapsing polyelectrolyte collect its counterions? Macromolecules 41, 9352–9358.

Lopez, C.G., 2019. Entanglement properties of polyelectrolytes in salt-free and excess-salt solutions. ACS Macro Letters 8, 979–983.

Lopez, C.G., 2020. Entanglement of semiflexible polyelectrolytes: Crossover concentrations and entanglement density of sodium carboxymethyl cellulose. Journal of Rheology 64, 191–204.

Lopez, C.G., Colby, R.H., Cabral, J.T., 2018. Electrostatic and hydrophobic interactions in nacmc aqueous solutions: Effect of degree of substitution. Macromolecules 51, 3165–3175.

Lopez, C.G., Colby, R.H., Graham, P., Cabral, J.T., 2017. Viscosity and scaling of semiflexible polyelectrolyte nacmc in aqueous salt solutions. Macromolecules 50, 332–338.

Lopez, C.G., Horkay, F., Schweins, R., Richtering, W., 2021. Solution properties of polyelectrolytes with divalent counterions. Macromolecules 54, 10583–10593.

Lopez, C.G., Matsumoto, A., Shen, A.Q., . Dilute polyelectrolyte solutions: recent progress and open questions .

Lopez, C.G., Richtering, W., 2018. Conformation and dynamics of flexible polyelectrolytes in semidilute salt-free solutions. The Journal of Chemical Physics 148.

Lopez, C.G., Richtering, W., 2019a. Influence of divalent counterions on the solution rheology and supramolecular aggregation of carboxymethyl cellulose. Cellulose 26, 1517–1534.

Lopez, C.G., Richtering, W., 2019b. Viscosity of semidilute and concentrated nonentangled flexible polyelectrolytes in salt-free solution. The Journal of Physical Chemistry B 123, 5626–5634.

Lopez, C.G., Richtering, W., 2021. Oscillatory rheology of carboxymethyl cellulose gels: Influence of concentration and ph. Carbohydrate Polymers 267, 118117.

Lopez, C.G., Rogers, S.E., Colby, R.H., Graham, P., Cabral, J.T., 2015. Structure of sodium carboxymethyl cellulose aqueous solutions: A sans and rheology study. Journal of Polymer Science Part B: Polymer Physics 53, 492–501.

Manning, G.S., 1969. Limiting laws and counterion condensation in polyelectrolyte solutions i. colligative properties. The journal of chemical Physics 51, 924–933.

Manning, G.S., 1996. Counterion condensation theory constructed from different models. Physica A: Statistical Mechanics and its Applications 231, 236–253.

Matsumoto, A., Ukai, R., Osada, H., Sugihara, S., Maeda, Y., 2022. Tuning the solution viscosity of ionic-liquid-based polyelectrolytes with solvent dielectric constants via the counterion condensation. Macromolecules 55, 10600–10606.

Muthukumar, M., 2002. Phase diagram of polyelectrolyte solutions: weak polymer effect. Macromolecules 35, 9142–9145.

Nandi, P., Das, B., 2005. Effects of concentration, relative permittivity, and temperature on the solution behavior of sodium carboxymethylcellulose as probed by electrical conductivity. The Journal of Physical Chemistry B 109, 3238–3242.

Nandi, P., Das, B., 2011. Electrical conductances of sodium carboxymethylcellulose in acetonitrile (1)+ water (2) mixed solvent media in the presence

of sodium chloride at 308.15 k. Journal of Chemical & Engineering Data 56, 2870–2876.

Nierlich, M., Boue, F., Lapp, A., Oberthür, R., 1985. Characteristic lengths and the structure of salt free polyelectrolyte solutions. a small angle neutron scattering study. Colloid and Polymer Science 263, 955–964.

Nierlich, M., Williams, C., Boué, F., Cotton, J., Daoud, M., Famoux, B., Jannink, G., Picot, C., Moan, M., Wolff, C., et al., 1979. Small angle neutron scattering by semi-dilute solutions of polyelectrolyte. Journal de Physique 40, 701–704.

Prabhu, V., Muthukumar, M., Wignall, G., Melnichenko, Y., 2001. Dimensions of polyelectrolyte chains and concentration fluctuations in semidilute solutions of sodium–poly (styrene sulfonate) as measured by small-angle neutron scattering. Polymer 42, 8935–8946.

Prabhu, V., Muthukumar, M., Wignall, G.D., Melnichenko, Y.B., 2003. Polyelectrolyte chain dimensions and concentration fluctuations near phase boundaries. The Journal of chemical physics 119, 4085–4098.

Ray, D., De, R., Das, B., 2016. Thermodynamic, transport and frictional properties in semidilute aqueous sodium carboxymethylcellulose solution. The Journal of Chemical Thermodynamics 101, 227–235.

Robinson, R.A., Stokes, R.H., 2002. Electrolyte solutions. Courier Corporation.

Rodrigues, R.K., de FC Martins, S., Naccache, M.F., de Souza Mendes, P.R., 2020. Rheological modifiers in drilling fluids. Journal of Non-Newtonian Fluid Mechanics 286, 104397.

Savary, G., Grisel, M., Picard, C., 2016. Cosmetics and personal care products. Natural polymers: industry techniques and applications , 219–261.

Schmidt, M., 1984. Combined integrated and dynamic light scattering by poly (γ-benzyl glutamate) in a helocogenic solvent. Macromolecules 17, 553–560.

Silva, A.F., Wood, T.A., Hodgson, D.J., Royer, J.R., Thijssen, J.H., Lips, A., Poon, W.C., 2022. Rheological design of thickened alcohol-based hand rubs. Rheologica acta 61, 571–581.

Truzzolillo, D., Bordi, F., Cametti, C., Sennato, S., 2009a. Counterion condensation of differently flexible polyelectrolytes in aqueous solutions in the dilute and semidilute regime. Physical Review E 79, 011804.

Truzzolillo, D., Cametti, C., Sennato, S., 2009b. Dielectric properties of differently flexible polyions: a scaling approach. Physical Chemistry Chemical Physics 11, 1780–1786.

Vink, H., 1982. Electrolytic conductivity of polyeiectrolyte solutions. Die Makromolekulare Chemie: Macromolecular Chemistry and Physics 183, 2273–2283.

Wagner, P., Różańska, S., Warmbier, E., Frankiewicz, A., Różański, J., 2023. Rheological properties of sodium carboxymethylcellulose solutions in dihydroxy alcohol/water mixtures. Materials 16, 418.

Yasuda, K., Armstrong, R., Cohen, R., 1981. Shear flow properties of concentrated solutions of linear and star branched polystyrenes. Rheologica Acta 20, 163–178.